Cancer Nanotechnology

RESEARCH Open Access

Lipo-MGN nanoparticle hypoxia attenuation-mediated single-dose radiotherapy- and pH/ROS-responsive T1 contrast magnetic resonance imaging in hepatocellular carcinoma

Reju George Thomas[1,2†], Subin Kim[1,2†], Raveena Nagareddy[2], Veena Vijayan[2], Ansuja Mathew Pullickal[2], Mee Sun Yoon[3], In Kyu Park[2] and Yong Yeon Jeong[1*]

[†]Reju George Thomas and Subin Kim have contributed equally to the manuscript

*Correspondence: yjeong@jnu.ac.kr

[1] Department of Radiology, Chonnam National University Medical School and Hwasun Hospital, 322 Seoyang-ro, Hwasun-eup, Hwasun-gun, Jeollanam-do 58128, Republic of Korea
[2] Department of Biomedical Sciences, Chonnam National University Medical School and Hospital, Gwangju, Korea
[3] Department of Radiation Oncology, Chonnam National University Hwasun Hospital, Chonnam National University Medical School, Gwangju, South Korea

Abstract

Tumor hypoxia is an important factor for developing resistance to radiation therapy (RT) and presents a bleak prognosis in cancer patients undergoing treatment for RT resistant hepatocellular carcinoma. Here, we present the synthesis of liposome-coated Mn_3O_4 (MGN) nanoparticles (Lipo-MGN) and investigation of their therapeutic potential with RT utilizing a HepG2 cancer model. According to in vitro research, Lipo-MGN effectively produced oxygen in the presence of H_2O_2 and significantly reduced the expression of HIF-1 in human HepG2 cells that were under hypoxic conditions. Lipo-MGN reversed the radio-resistance brought on by hypoxia and increased cell damage. When Lipo-MGN and RT were administered together in a HepG2 xenograft mice model, the tumor growth was delayed more than with RT alone. As determined by MR imaging, liposome-MGN also exhibited T1 contrast enhancement in tumor. According to these findings, Lipo-MGNs may increase the impact of RT by focusing tumor hypoxia. Hypoxic, radioresistant HepG2 cancer may be treated with Lipo-MGN in clinical studies.

Keywords: Liposome, Manganese oxide, Cancer, Nanoparticle, Hypoxia

Introduction

Hepatocellular carcinoma (HCC) is the fifth most prevalent type of malignant tumor in the world. Approximately 700,000 people are diagnosed annually with liver cancer in the United States alone (Xu et al. 2021). The curative treatment for HCC has been liver transplantation, surgical resection and radiofrequency ablation (Park et al. 2020; Sayan et al. 2019). The radiation generated from radioactive source or X-ray, Gamma ray generator have high energy and short wavelength which when directed to region affected by tumor will result in direct damage or nucleic acid degeneration leading to tumor shrinkage. The disadvantage of radiation therapy is reduction in efficiency due to hypoxia in HCC because tumor nodules consume a high amount of oxygen. Therefore, HCC is

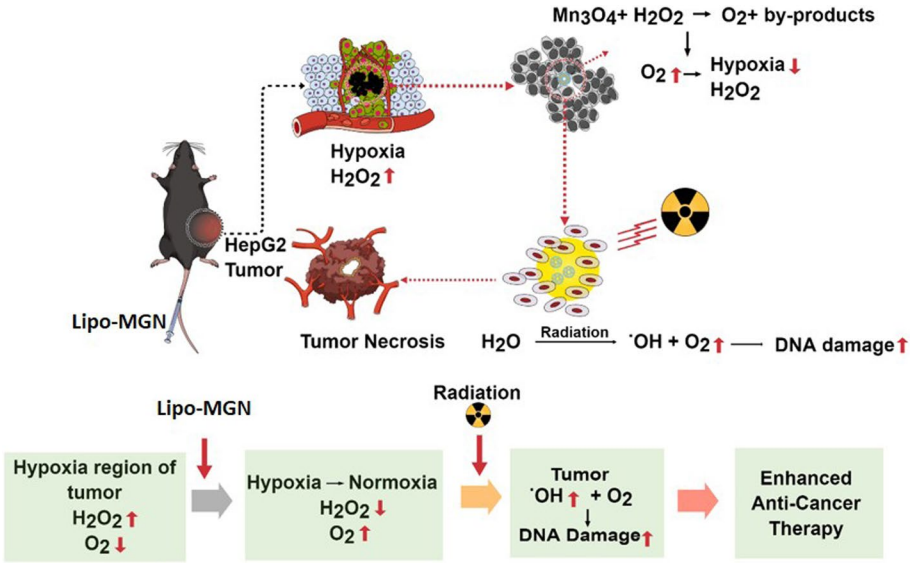

Scheme 1 Intravenous injection of Lipo-MGNs reduced hypoxia in tumours and promoted cell death in radiation therapy

considered to be one of the most hypoxic tumor (Elbanna et al. 2021; Chen and Lou 2017). To overcome this issue therapeutic agents can be introduced to convert hypoxic microenvironment to normoxic microenvironment such as manganese oxide nanoparticle which has the ability to decompose in presence of reactive oxygen species and glutathione to produce oxygen (Yang et al. 2017; Scheme 1).

Hypoxia can promote tumor progression and induce RT resistance. HCC is considered to be a hypoxic tumor (Chen and Lou 2017). The direct effect of hypoxia can be seen in the gene expression level of hypoxia inducible factor-1 (HIF-1) which will increase with hypoxia level and decrease with oxygen level due to hydroxylation. Angiogenesis, proliferation, invasion, metabolism, metastasis, and resistance to therapy are only a few of the ways that HIF-1 genes contribute to the development and spread of tumors and cancer. Radiation resistance due to hypoxia is a major issue facing the clinical outcome of RT (Sorensen and Horsman 2020).

MGN is the type most commonly modified for the generation of oxygen (Prasad et al. 2014). MnO_2 nanoparticles have been loaded in hyaluronic acid (HA)-based nanoparticles to target tumor-associated macrophages (TAMs) and reduce hypoxia in tumors to improve chemoresistance caused by hypoxia. Additionally, HA-MnO_2 nanoparticles showed T1 and T2 contrast ability in tumor MR imaging (Song et al. 2016). Albumin MnO_2 nanoparticles were able to reduce hypoxia and downregulate HIF1-alpha. Breast tumor growth was greatly reduced when albumin MnO_2 nanoparticles and radiation therapy were used in combination (Prasad et al. 2014). Fucoidan-coated MnO_2 nanoparticles Fuco-MnO_2-NPs effectively produced oxygen in the presence of H_2O_2 and significantly reduced HIF-1 expression under hypoxic conditions in human pancreatic cancer cells (Shin et al. 2018).

MGN has the advantages that it has over other manganese oxide types, such as MnO, MnO_2 and Mn_2O_3, for generating more molecular oxygen. Mn_3O_4 has a higher

ROS-scavenging ability owing to the double oxidation states of Mn^{3+} and Mn^{2+}, which can lead to the conversion of ROS ($O_2^{\cdot-}$ and $^{\cdot}OH$) to molecular oxygen released in inflammation (Choi et al. 2022; Yao et al. 2018). There are a few reports about Mn_3O_4 nanoparticles (MGNs) for cancer therapy. Doxorubicin-loaded, serotonin–stearic acid-based Mn_3O_4 nanocuboids (Jain et al. 2020) for HCC therapy and Au@ Mn_3O_4 magneto-plasmonic nanoflowers (Ijaz Dar et al. 2020) for photothermal cancer therapy have been reported.

PEG (polyethylene glycol) is hydrophilic and has also been shown to protect nanoparticles from phagocytosis by the reticuloendothelial system in the liver so that blood circulation increases, mediating more bioavailability to the tumor region. We used PEGylated liposomes to load MGN to increase the solubility of hydrophobic Mn_3O_4 and increase bioavailability. To our knowledge, no other work has reported PEGylated liposome-loaded Mn_3O_4. Here, we synthesized PEGylated liposome-loaded Mn_3O_4 to attenuate hypoxia in HepG2 cancer cells for radiosensitization and contrast-enhanced TI-weighted MR imaging.

Materials and methods

Synthesis of manganese oxide nanoparticles and Lipo-MGNs

1-Dodecanethiol-stabilized hydrophobic Mn_3O_4 nanoparticles were prepared as previously described (Choi et al. 2022). The film hydration process was used to make liposomes. Briefly, 1.5:1.5:1 (weight ratio) of DSPE-PEG, DPPC, and cholesterol were added to the appropriate solvents (methanol for DSPE-PEG, DPPC, and cholesterol) and combined in a vortex for 2 min in a glass vial. Thin film hydration was formed in a vacuum chamber at room temperature by evaporation of the aforementioned solvents. Then, the film was hydrated using 1 ml of distilled water and heated in a glass vial for 30 min at 60 °C to promote the formation of multivesicular liposomes, which are heterogeneous in nature. To make Mn_3O_4-loaded liposomes (Lipo-MGN), we prepared 1.5 times (1.5×) the concentration of lipids and added 1.5 mg of Mn_3O_4 during thin film formation. Finally, the Lipo-MGNs were probe-sonicated for 10 min. Unloaded Mn_3O_4 was removed by dialysis in 4 °C for 2 h.

Characterization of the Lipo-MGNs

Using a Zetasizer instrument, the size and Zeta potential of Lipo-MGN were examined to calculate the surface charge (Nano-Z590, Malvern Instruments, Worcestershire, UK). Using field emission transmission electron microscopy, the size and morphology were validated (FE-TEM). For liposome drug loading capabilities, Mn_3O_4 encapsulation and loading were studied using inductively coupled atomic emission spectroscopy (ICP-AES) and thermogravimetric analysis (TGA).

Cell viability of Lipo-MGNs

The MTS assay was used to determine the cell viability of Lipo-MGNs and MGNs in the NIH3T3 cell line. 96-well plates were seeded with a total of 10^4 cells per well and cultured for one day at 37 °C in a CO_2 incubator. Lipo-MGN effect in HepG2 after radiation (10 Gy) was studied by MTS assay. HepG2 cells from the human liver cancer cell line were seeded in 35 mm petri dish from Lab-Tek2 (New York, USA) at a density of

10^5 cells and incubated for one day at 37 °C in a humidified CO_2 atmosphere. The Lipo-MGNs and MGNs viability was examined in triplicate across the concentration range of 100–0.78 μg/ml. After the cells had been treated for 24 h, they were incubated for another 24 h in fresh media before 20 μl of the MTS reagent was added and incubated for 3–4 h in each well. In case of Lipo-MGN treatment in HepG2 cell line, cells were irradiate with 10 Gy of radiation before MTS reagent was added. With the aid of a microplate reader, the absorbance was calculated.

Cell uptake of liposomes by human liver cancer cell line|

HepG2 cells from the human liver cancer cell line were seeded in 8-well chamber slides from Lab-Tek2 (New York, USA) at a density of 5×10^4 and incubated for one day at 37 °C in a humidified CO_2 atmosphere. HepG2 cells were cultured in Dulbecco's modified Eagle's medium (DMEM), which contains 10 vol% FBS and 1 vol% penicillin–streptavidin–amphotericin B (Gibco Anti-Anti (100×), USA). Following a 24-h incubation period, 100 μg/ml of DiD dye, a lipophilic carbocyanine dye-loaded liposome, was added to each well. The cells were then incubated after receiving these treatments. The cells were incubated for 24 h before being rinsed with PBS to remove any excess dye and fixed with a 4% formaldehyde solution. Using a confocal microscope, the cells were captured (Zeiss LSM 510, Oberkochen, Germany).

In vitro hypoxia assay

We used Image-iT™ Green Hypoxia Reagent (ThermoFisher, Massachusetts, USA) to check the conversion from hypoxia to normoxia in the HepG2 cell line. When the oxygen concentration is decreased (below 5%) in live HepG2 cells, the fluorogenic compound in the hypoxic reagent is activated and sustains the fluorescence. We measured the hypoxia level based on the intensity of fluorescence.

HepG2 cells were cultured in 24-well plates in a humidified CO_2 chamber at 37 °C for 1 day. Dulbecco's modified Eagle's medium (DMEM) containing 10 vol% FBS and 1 vol% penicillin–streptavidin–amphotericin B (Gibco Anti-Anti (100×), USA) was used for HepG2 cells. After 24 h of incubation, the plate was placed in a hypoxia chamber (hypoxia chamber spec) for overnight incubation. Lipo-MGN was treated with 25–100 μg/ml [Mn] and incubated for another 6 h. Cells were washed with PBS, treated with hypoxia reagent at a 5 μM concentration and incubated at 5% CO_2 and 37 °C for 4 h. The cells were washed again with PBS and observed under a fluorescence microscope.

In vitro T1-weighted MR imaging of Lipo-MGNs

To evaluate the effects of pH and ROS on Lipo-MGN dissociation, we conducted T1-weighted MR imaging by 3 T clinical MRI instrument (Magnetom Tim Trio, Siemens Medical Solutions, Erlangen, Germany) at different pH and H_2O_2 values using Lipo-MGNs. Lipo-MGN at 0.72 mg Mn/mL was serially diluted to 0, 0.25, 0.5, 1, and 2 mM Mn concentrations, and T1-weighted MR imaging was conducted.

Animal tumor model

Male BALB/c nude mice (18–20 g, 5 weeks old) or female BALB/c nude mice (18–20 g, 5 weeks old) were purchased from Jungang Lab Animal Inc. in Korea for biodistribution

research, in vivo tumor reduction investigations, and animal toxicity studies. The Chonnam National University Medical School Research Institutional Animal Care and Use Committee approved the use of animals in the study, and it was conducted in accordance with the National Institutes of Health Guide for the Care and Use of Laboratory Animals (CNU IACUC-H-2019-6). HepG2 tumors were induced in mice by subcutaneous injection of 106 HepG2 cells close to the hind limb. We utilized the formula $L * B^2/2$ to determine the tumor's volume, where L stands for the tumor's length (major axis) and B for its width (minor axes).

In vivo *biodistribution of Lipo-MGNs by ICP-MS*

Lipo-MGN (in PBS, 200 ul) at a concentration of 0.15 mg [Mn_3O_4]/kg (7.5 mg/kg of Mn_3O_4) was injected into each mouse intravenously through the tail vein of HepG2 tumor-bearing mice after HepG2 tumors attained a size of around 5–7 mm (after around 15 days). At the 8- and 24-h time points, organs were extracted and added to 3 ml of aqua regia and mixed with 27 ml of distilled water to make a 10% aqua regia:water mix and submitted for ICP-MS. ICP-MS was performed in a Varian 820 ICP Mass Spectrometer (Varian Medical Systems, UK).

In vivo T1-weighted MR imaging

For in vivo MR imaging, male BALB/c nude mice (5–6 weeks old, 20 g) were used. Subcutaneous injections of HepG2 cells at a density of at least 1×10^7 cells were made in DMEM-cultured cells at 37 °C and 5% CO_2. Mice were anesthetized using isoflurane (Forane soln. Abbot, USA). T1-weighted MR imaging (M7™ Compact MRI System (AspectImaging, Shoham, Israel) was performed as follows: TR/TE: 400/10 ms TI: 100 ms, echo train length: 10, flip angle: 150°, field of view: 4 cm, number of slices: 15, slice thickness: 1.5 mm, interslice gap: 0 mm, and matrix: 256×210. When the tumor size reached 100–150 mm^3, MR imaging was obtained for Lipo-MGNs in PBS at pre-injection and 3, 6, 8, and 24 h post-injection.

Cytotoxicity analysis by radiation using FDA/PI assay

HepG2 cells (5×10^4) were seeded in confocal petri dishes (Lab-Tek2, USA) and cultured in DMEM at 37 °C with 5% CO_2 in a humid atmosphere. After 24 h incubation, 100 µg/ml Lipo-MGN was added and incubated for 6 h. The wells were washed 3 times with warm PBS and then irradiated at 3 Gy and 10 Gy. After radiation, the Lipo-MGN sample was treated with 8 µl of FDA (4 µM) and PI (0.5 µM) dissolved in PBS for 5 min at room temperature. With Texas Red® dye filter for PI and a fluorescein bandpass filter for FDA, the wells were observed under a fluorescence microscope.

Oxygen generation of the Lipo-MGNs

The O_2 generated by Lipo-MGNs was measured using an O_2-ADPT Oxygen Adapter (Microelectrodes Inc., USA). Briefly, 15 ml of a solution of 1 mg/ml Lipo-MGN was prepared, and H_2O_2 was added to a final concentration of 1 M. The oxygen level was measured in mg/l dissolved oxygen in a solution of Lipo-MGN + H_2O_2. Measurements were taken every 5 min and measured for up to 60 min.

mRNA isolation, cDNA conversion, and quantitative real-time PCR HIF alpha PCR study

HepG2 cells were seeded in 6-well plates and cultured in DMEM in a 5% CO_2 incubator at 37 °C in a humidified environment. Then, Lipo-MGN was added at a concentration of 100 µg/ml and incubated for 6 h under normoxic and hypoxic conditions. Cells were washed thoroughly with ice-cold PBS before mRNA extraction. Before extracting the mRNA from cells, cells were lysed using cell lysis buffer at 0 °C to maintain mRNA integrity. Total RNA was isolated using an RNeasy kit (QIAGEN, Germany).RT-PCR was done by SYBR Green PCR master mix (Applied Biosystem, UK).

Immunohistochemical detection of tumor hypoxia

HepG2 tumor BALB/c nude mice ($n=3$) were intravenously injected with Lipo-MGNs at a dose of 7.5 mg/kg. Hypoxia detection assay (Hypoxyprobe-1 plus kit, Hypoxyprobe Inc., USA) was carried out using the kit's specified methodology for ex vivo tissue staining of hypoxia. One day after injection of Lipo-MGN, pimonidazole hydrochloride was injected intraperitoneally. Pimonidazole hydrochloride will accumulate in tumors within 60 min. After 60 min, tumor tissue was collected and preserved for histological examination in 10% neutral buffered formalin solution (Sigma Aldrich, USA).

In vivo radiation treatment

HepG2 xenograft liver cancer model in BALB/c mice was created. Four groups of mice ($n=5$ each group) were used. (a) The non-radiation control group (NC), (b) the radiation only (RO) group, (c) the radiation high-concentration Lipo-MGN (RH) group, and (d) the radiation low-concentration Lipo-MGN (RL) group. When the tumors reached volume of about 100 mm^3, treatment started. The mice were held in a restrainer in a low-dose-rate research radiator (Gammacell, 40 exactor, Theratronics, ON, Canada). For RH and RL groups i.v. administration of Lipo-MGNs were given at 7.5 mg/kg [MGN] and 3.75 mg/kg [MGN], respectively. The tumors were irradiated locally with 6 Gy, 10 min for RO, RH and RL group. Vernier callipers were used to assess the tumor size over time in two dimensions, and the tumor volume was computed using the formula $V=[(\text{length}) \times (\text{width})^2]/2$. The animals were killed at the conclusion of the trial, and the tumor masses were removed and weighed. TUNEL assay was used to determine the level of apoptosis in tumor tissue after radiation. After fixing tumor tissue after 4% PFA, the tissue was deparaffinized. Using the ApopTag® Peroxidase in Situ Apoptosis Detection Kit (Millipore, Burlington, MA, USA), TUNEL staining was carried out.

Results

Lipo-MGN characterization

Lipo-MGN was successfully synthesized. A final hydrodynamic size of 150 nm and a negative Zeta potential were noted. In EDS elemental analysis, the total manganese content was found to be 34.48%, and the oxygen content was 65.52%. The encapsulation and loading efficiencies were 25% and 12.10%, respectively, for the 300-kDa filtration sample compared to 30% and 10.96% for the 6–8 kDa sample. We used the 300-kDa dialysis method for purification of Lipo-MGN, as it has 50 nm pores that can effectively filter

out unloaded MGN nanoparticles, which have an average size of 20–30 nm. Thus, only loaded lipo-MGNs could be collected for further experiments. This is the reason why 300 kDa had a better loading efficiency than 6–8 kDa and was selected (Fig. 1).

Lipo-MGN cellular uptake and viability

The viability of Mn_3O_4 and Lipo-MGNs was measured by MTS assay at concentrations up to 100 µg/ml in the NIH3T3 cell line (Fig. 2A).

We can see the toxicity of MGN starting from the 6.25 µg/ml concentration, decreasing below 80% cell viability and reaching up to 55% cell viability at 100 µg/ml compared to Lipo-MGN, which showed 80% cell viability at 100 µg/ml. This result can be attributed to liposomes, which are biocompatible and protect cells from the direct interaction of manganese oxide nanoparticles, which induce toxicity from oxidative stress. Fluorescence analysis of DiD-loaded liposomes showed high uptake of Lipo-DiD at 100 µg/ml (Fig. 2B). Lipo-MGN effect in HepG2 after radiation (10 Gy) was studied by MTS assay. Data show 50% cell toxicity after radiation compared to the control owing to the conversion of hypoxia to normoxia by lipo-MGN (Fig. 2C). LogIC50 was calculated to be 2.284 based on log-dose versus response curve. IC50 value calculated was 192.3 ug/ml of Lipo-MGN after radiation (Fig. 2D).

In vitro *hypoxia study*

Our study aimed to convert the hypoxic state of the tumor microenvironment to a normoxic state to promote the RT effect. We used the HepG2 cell line incubated in a

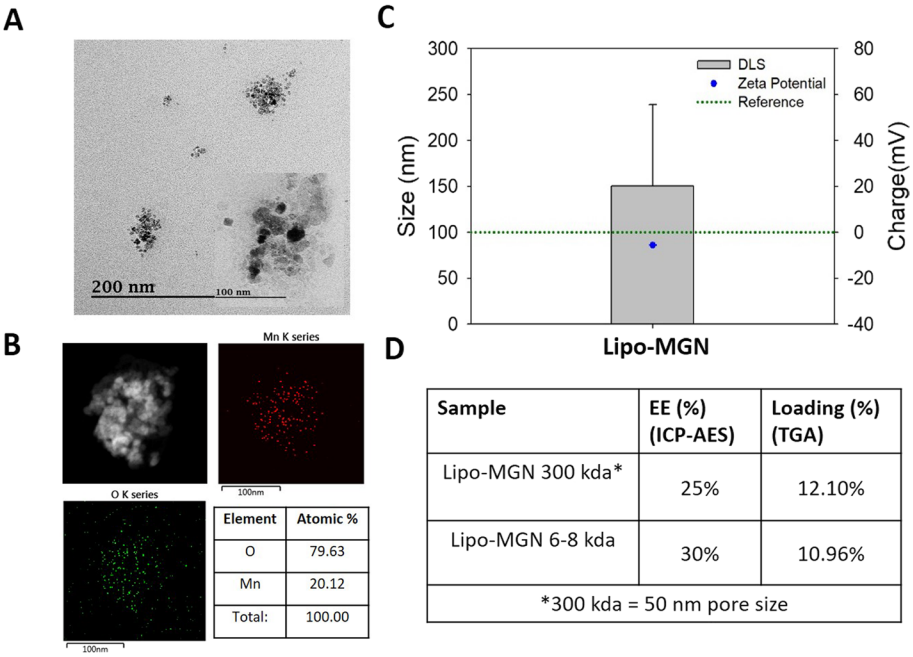

Fig. 1 Lipo-MGN characterizations. **A** FE-TEM imaging of the Lipo-MGNs. Manganese oxide nanoparticles are embedded in the hydrophobic region on liposomes. The inset image shows MGN loaded in liposome. **B** Elemental analysis of Lipo-MGNs by EDX showing the presence of manganese and oxygen. **C** DLS and Zeta potential analyses of the Lipo-MGNs. **D** Encapsulation and thermogravimetric analyses of Lipo-MGNs after purification at 300 kDa and 6–8 kDa

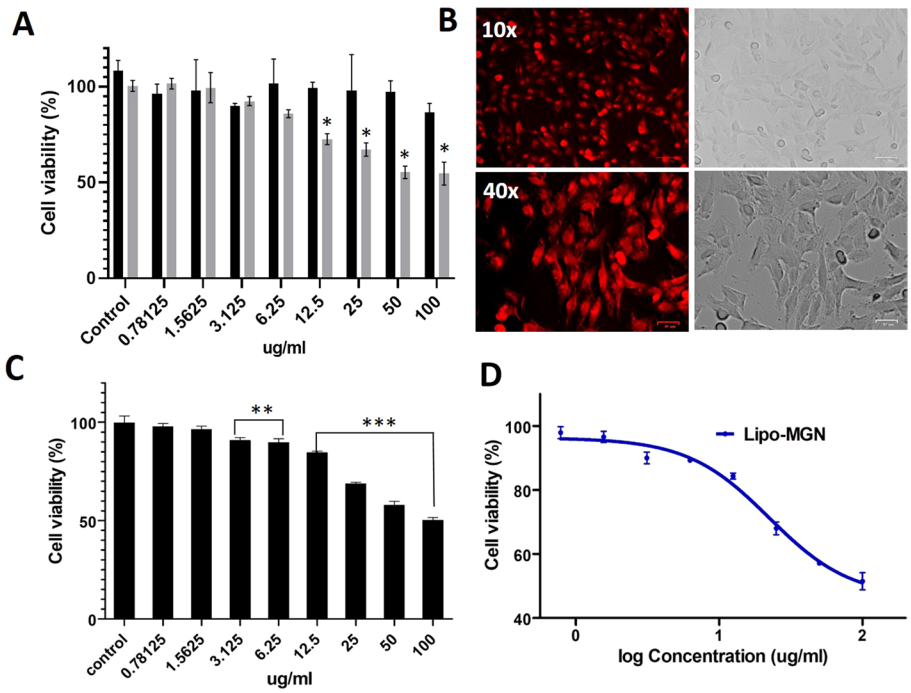

Fig. 2 Cell viability by MTS assay and cell uptake analysis. **A** MTS assay showing the viability of Lipo-MGNs (black bar) and MGN (grey bar) in NIH3T3 cell line. **B** Lipo-DiD uptake in Hep-G2 cells. **C** MTS assay showing viability of Lipo-MGNs after radiation in HepG2 cell line. **D** Log-dose versus response curve of Lipo-MGNs after radiation in HepG2 cell line. MTS assay data show the mean cell viability of quadruplicate samples ± SD. A two-tailed probability value (*P*) < 0.05 was considered statistically significant. **P* < 0.05 relative to Lipo-MGN. ***P* < 0.01 and ****P* < 0.001 relative to the control

hypoxia chamber (CO_2 5% and O_2 1%) and treated them with Lipo-MGN at different concentrations to produce oxygen and reinstate normoxia. We used Image-IT™ green hypoxia reagent to check the conversion from hypoxia to normoxia. We observed that 100 µg/ml Lipo-MGNs in hypoxia maximally suppressed fluorescence compared to the control. In FACS analysis, we can see almost 20% suppression of fluorescence for 100 µg/ml Lipo-MGN compared to the hypoxia group with no nanoparticles. At decreasing concentrations up to 25 µg/ml, the fluorescence increased (40% for 50 µg/ml, 68% for 25 µg/ml). The hypoxia group had 90% fluorescence. These data clearly showed the role of Lipo-MGNs in generating oxygen that interacts with fluorogenic compounds in the Image-iT™ Green Hypoxia Reagent (Fig. 3).

In vitro *hypoxia cell toxicity study*

As per the in vitro hypoxia assay, 100 µg/ml Lipo-MGN generated sufficient oxygen to bring hypoxic HepG2 cells to normoxia. This oxygenation is very important in the RT of HCC, as oxygen prevents the repair of double-strand breaks in DNA, leading to cell death. To validate this theory, we performed a live/dead assay after RT of HepG2 cells treated with Lipo-MGNs at 3 and 10 Gy. Live/dead assay is a method to evaluate the cell viability using green dye (FDA) representing live cells and red dye (PI) to represent dead cells. We observed that at lower radiation (3 Gy), propidium iodide fluorescence started to appear to be caused by cell death in the hypoxia group, whereas normoxic cells were

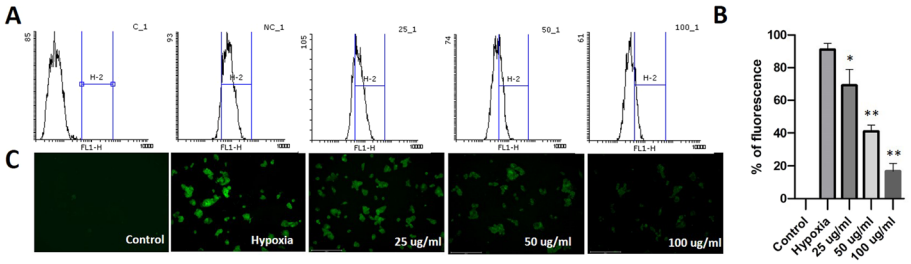

Fig. 3 In vitro hypoxia assay in HepG2 cells using Lipo-MGNs by the Image-iT™ Green Hypoxia Reagent. **A** FACS analysis showing the fluorescence level of the HepG2 cell line after treatment with the Image-IT probe for the control, hypoxia, and 25, 50, 75, and 100 µg/ml groups. **B** Quantification of FACS data. **C** Qualitative fluorescent image of HepG2 cells. The data are presented as the mean ± standard deviation with number of samples (n) = 3. The mean % of fluorescence level showed significant differences between the hypoxia and Lipo-MGN treated groups (25, 50 and 100 µg/ml) as analyzed by the Student's unpaired t-test. A two-tailed probability value (P) less than 0.05 was considered statistically significant. *indicates $P < 0.05$, ** indicates $P < 0.0001$

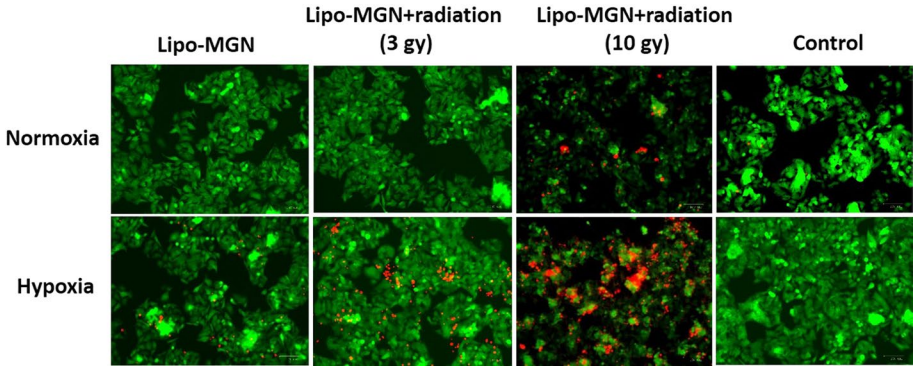

Fig. 4 In vitro cell toxicity after radiation by live/dead assay. Lipo-MGN with radiation (Lipo-MGN + radiation) at 3 and 10 gy radiation dose treated in normoxic and hypoxic cell lines showed a higher level of red fluorescence (PI) indicating cell death compared to Lipo-MGN without radiation (Lipo-MGN) and control

relatively viable. At 10 Gy radiation, almost 80% of the cells were killed even in the normoxia group. Compared to the normoxia group, hypoxia resulted in more cell death in the 3 and 10 Gy groups, which may be due to toxicity related to the hypoxic environment (Fig. 4).

In vitro *T1-weighted MR imaging of Lipo-MGNs*

For checking the possibility of MR imaging using Lipo-MGN, we tested T1 contrast at different pH (7.4 and 6.8) and H_2O_2 (0.1 mM and 1 mM) values. T1 contrast signal intensity incrementally increased as the pH value decreased and as the H_2O_2 concentration increased (Fig. 5A). The mean signal intensity significant differences between three groups at different Mn concentrations as analyzed by repeated measure ANOVA test are shown in Fig. 5B. T1 relaxivity (r1) was found highest for pH 6.8 + 1 mM H_2O_2 at 2 mM [Mn] concentration of Lipo-MGN ($r1 = 4.02\ mM^{-1}\ s^{-1}$) compared to pH 7.4 + 0.1 mM H_2O_2 at 2 mM [Mn] concentration of Lipo-MGN ($r1 = 0.18\ mM^{-1}\ s^{-1}$). This data validates that both pH and ROS played important roles in the dissociation of MGN to Mn ions, contributing to the T1 signal intensity shown in the data. Table comparing

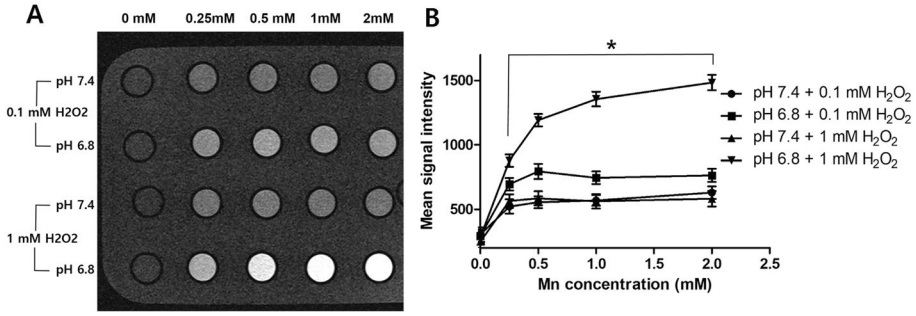

Fig. 5 In vitro MRI study of Lipo-MGN at different H_2O_2 concentrations and pH values. **A** T1-weighted MR contrast images of Lipo-MGNs from 0 to 2 mM concentrations at pH 6.8–7.4 and at 0.1 mM and 1 mM H_2O_2 concentrations. **B** Graph plotting the contrast signal intensity of Lipo-MGNs from 0 to 2 mM concentrations at pH 6.8–7.4 and at 0.1 mM and 1 mM H_2O_2 concentrations. The data are presented as the mean ± standard error of the mean with number of samples (n) = 3. The mean signal intensity significant differences between three groups at different Mn concentration as analyzed by repeated measure ANOVA test and in the post hoc analysis by Tukeys test (pH 7.4 + 0.1 mM H_2O_2 vs. pH 6.8 + 1 mM H_2O_2: *P < 0.05)

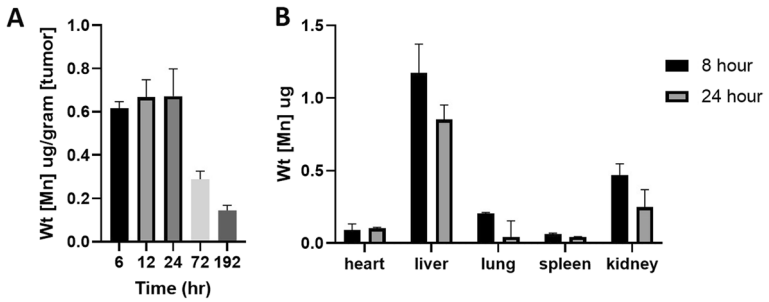

Fig. 6 Ex vivo biodistribution of Lipo-MGNs by ICP-MS analysis in **A** HepG2 tumors at different time points and **B** organs at 8- and 24-h time points. The data are presented as the mean ± standard deviation with number of samples (n) = 5

relaxation time (T1), relaxation rate (R1) and relaxivity (r1) of each group is included in Additional file 1: S2.

Ex vivo biodistribution by ICP-MS

When HepG2 tumors reached approximately 5–7 mm in size (after approximately 15 days), Lipo-MGN (in PBS, 200 µl) at a concentration of 0.15 mg [Mn_3O_4]/kg (7.5 mg/kg of Mn_3O_4) was intravenously injected into each mouse through the tail veins of HepG2 tumor-bearing mice. At 8- and 24-h time points, the organs were extracted and added to 3 ml of aqua regia and mixed with 27 ml of distilled water to make a 10% aqua regia:water mixture and submitted for ICP-MS.

To measure the manganese oxide content in organs and tumors after i.v. injection of Lipo-MGNs, ex vivo ICP-MS analysis was performed at different time points. Tumors were extracted at 6, 12, 24, 72 and 192 h, and the highest accumulation was found at the 24-h time point and had decreased by the 72-h time point, indicating elimination of Lipo-MGNs from the tumor region (Fig. 6A). The MR imaging data also validate this result. The highest accumulation levels of manganese oxide were found in the liver and kidney at the 8-h time point (Fig. 6B). After 24 h, there was a decrease in manganese

oxide, which can be attributed to increased accumulation in tumors and natural elimination by the reticuloendothelial system (RES) in the liver and kidney.

In vivo MR imaging

For in vivo MR imaging, mice bearing HepG2 tumors were injected intravenously with Lipo-MGNs (7.5 mg/kg), and the mice were then scanned using MR technique. After Lipo-MGN injection, the MRI signal intensity of HepG2 tumors ($n=4$) steadily decreased over time. At one day after injection, the contrast enhancement (signal decrease) was seen to be at its peak (Fig. 7).

Oxygen generation and HIF alpha PCR studies

Oxygen generated by Lipo-MGNs was measured using an O_2-ADPT Oxygen Adapter (Microelectrodes Inc., USA). Briefly, 15 ml of a solution of 1 mg/ml Lipo-MGN was prepared, and H_2O_2 was added to a final concentration of 1 M. The oxygen level was measured in mg/l dissolved oxygen in a solution of Lipo-MGN + H_2O_2. Measurements were taken every 5 min and measured for up to 60 min. The oxygen release in mg/L reached

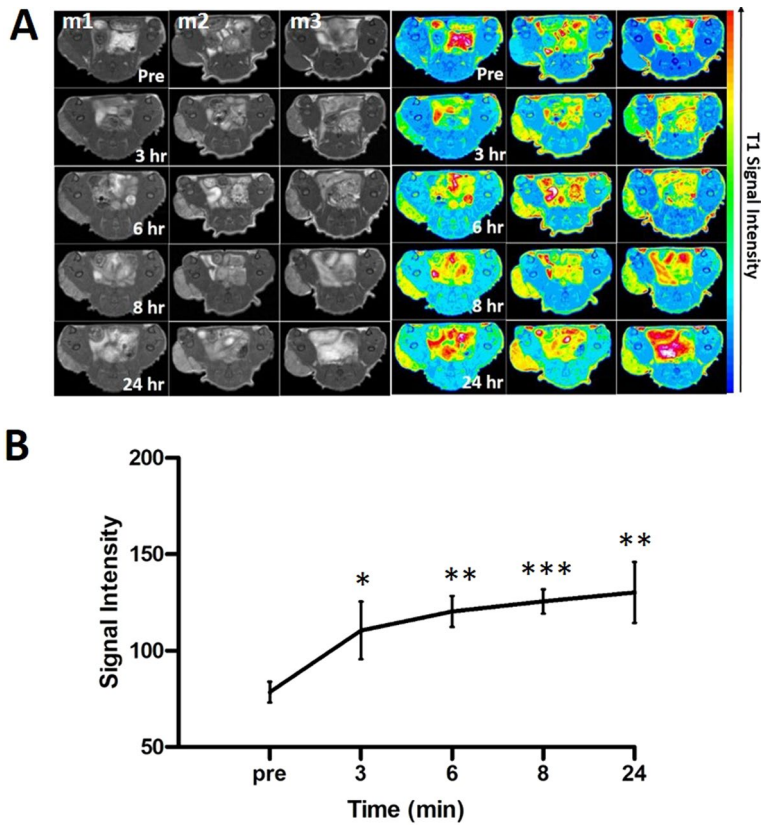

Fig. 7 In vivo MR imaging of nu BALB/C mice injected with Lipo-MGNs at different time points. **A** T1-weighted MR contrast images of mice 1, 2 and 3 (m1, m2, m3) at different time points. **B** T1 contrast intensity ratios pre-injection and post-injection of Lipo-MGNs. The data are presented as the mean ± standard deviation with number of samples (n) = 3. The mean signal intensity showed significant differences between the pre-injection and post-injection time points (3, 6, 8 and 24 h) as analyzed by the Student's unpaired t-test. A two-tailed probability value (p) < 0.05 was considered statistically significant. *Indicates $P<0.05$, ** indicates $P<0.01$, *** indicates $P<0.001$

10 mg/L immediately after mixing with H_2O_2 and reached up to 38 mg/L in 60 min. Then, the release reached the threshold most likely when the Lipo-MGN reaction with H_2O_2 released oxygen and the oxygen escaping from solution reached equilibrium. In response to oxygen release in the HepG2 cancer cell line, hypoxia inducible factor-1 alpha is degraded by oxygen (Fig. 8A). To prove this effect, we conducted HIF-1α mRNA quantification in the presence of Lipo-MGNs by PCR. Compared to the control, HepG2 cells under hypoxia showed a fivefold increase in mRNA levels, and due to the oxygenation capability of Lipo-MGN, the HIF-1α mRNA level in the Lipo-MGN group was comparable to that of the control group. This prove the oxygenation capability of Lipo-MGN and therefore better radiation sensitization in hepatocellular carcinoma (Fig. 8B).

In vivo tumor reduction by radiotherapy

HepG2 tumors were grown in BALB/c mice. As shown in the graph of T1 contrast signal intensity, the peak intensity was reached at the 24-h time point, which we took as the time point to use for radiotherapy after the Lipo-MGN dosage. The tumor size after RT was measured and plotted, as shown in Fig. 9A. The tumor size of the RH group was significantly lower than that of the RO group. This can be attributed to the toxic effect caused by DNA damage caused by radiation and oxygen-mediated DNA repair prevention. The effect of oxygen was confirmed by the results of the RL group, which had a lower concentration of Lipo-MGN and therefore lower oxygen release. A survival study of mice after radiation therapy was conducted, with the last mice in the RH group surviving for more than 85 days compared with 38 days in the control (Additional file 1: S4).

Immunohistochemical detection of tumor hypoxia was done by hypoxia detection assay. DAB staining was performed to view the anti-HRP secondary antibody binding. It is seen from the data that compared to control, Lipo-MGN low and high concentration

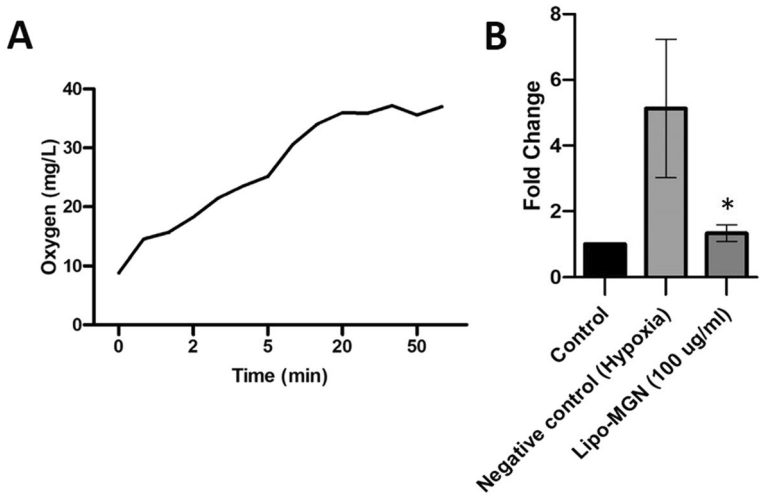

Fig. 8 In vitro oxygen release study of Lipo-MGNs. **A** Reaction scheme showing the reactivity of Lipo-MGNs towards H_2O_2 for the production of oxygen. **B** RT–PCR analysis of HIF-1α mRNA expression after Lipo-MGN treatment in the HepG2 cell line. HIF-1α mRNA is degraded by the oxygen released by Lipo-MGN. The data are presented as the mean ± standard deviation with number of samples (n) = 3. The mean fold change mRNA expression showed significant differences between the hypoxia and Lipo-MGN (100 µg/ml) treated group as analyzed by the Student's unpaired t-test. A two-tailed probability value (p) less than 0.05 was considered statistically significant. *Indicates $p < 0.05$

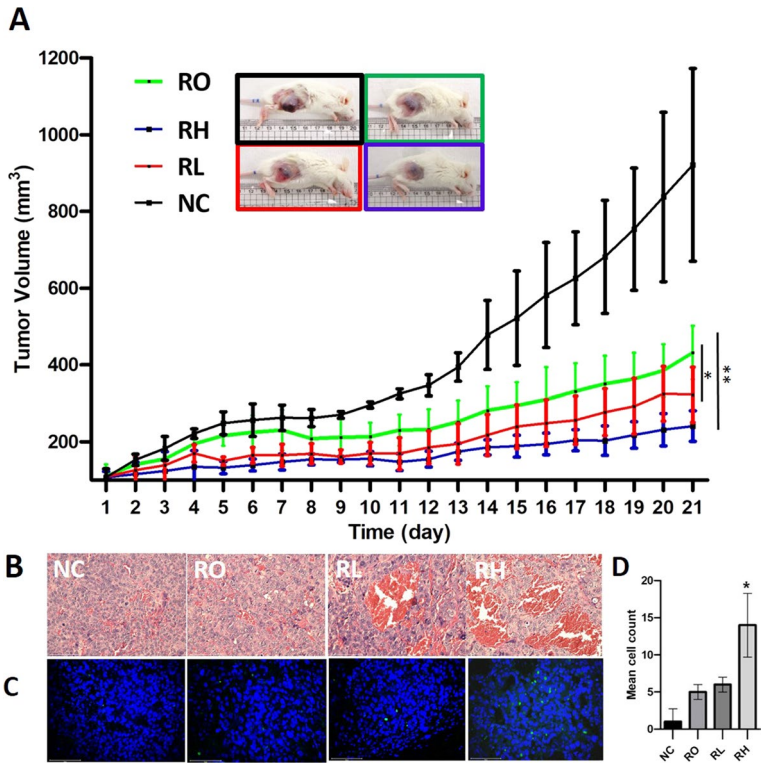

Fig. 9 In vivo tumor reduction by radiotherapy. **A** Tumor volume plotted against time. **B** H&E staining of tumor tissue for the NC, RO, RL, RH groups after radiation. **C** TUNEL assay of the NC, RO, RL, RH groups after radiation. **D** Mean cell count of TUNEL-positive cells (green fluorescence) is represented as graph for the NC, RO, RL, RH groups after radiation. The data are presented as the mean ± standard deviation with number of samples (n) = 5 for tumor volume against time and n = 3 for mean cell count of TUNEL-positive cells. The mean tumor volume showed significant differences between the RO and Lipo-MGN-treated group (RL and RH) at day 21, as analyzed by the Student's unpaired t-test. The mean cell count of TUNEL-positive cells showed significant difference between the RH and RL, as analyzed by the Student's unpaired t-test. A two-tailed probability value (p) less than 0.05 was considered statistically significant. *Indicates $p < 0.05$, ** indicates $p < 0.0001$

is having lesser staining for both DAB and FITC, which indicate lesser pimonidazole adducts. This experiment show that Lipo-MGN will increase oxygen and prevent formation on pimonidazole adduct in tumor (As shown in Additional file 1: Figure S5).

Ex vivo toxicity analysis was performed using H&E staining and TUNEL staining to check the effect of radiation with and without the presence of Lipo-MGNs. The RH group showed more TUNEL-positive cells than the RL and RO groups. H&E staining also clearly showed cells that were damaged due to radiation in the RH and RL groups compared to the RO and NC groups. These results suggest that Lipo-MGNs at higher concentrations can be re-oxygenated in tumors both in vitro and in vivo (Fig. 9B, C).

Discussion

We prepared PEGylated Lipo-MGNs to generate oxygen and convert the hypoxic HCC microenvironment to a normoxic microenvironment. We also used manganese oxide in Lipo-MGNs to obtain T1 contrast MR images. Mn ions are biocompatible materials and provide bright T1-contrast MR imaging. Following incubation in acidic media, r_1 increased due to the evolution of free Mn^{2+} (Gale et al. 2015; Cai et al. 2019). The MRI

data in our study also clearly show how manganese oxide dissociates in the presence of ROS and low pH and forms manganese ions, which are responsible for the TI contrast shown in MRI.

An in vitro cytotoxicity study showed that Lipo-MGNs are more biocompatible than bare manganese oxide nanoparticles, which is good if the circulation time to reach peak bioavailability in tumors is 24 h. The in vitro MRI results showed the relationship between pH and ROS levels in the MR T1 contrast level. When the nanoparticles are taken up by cell, they are transported to lysosomes and endosomes, where the pH is low. Inorganic D-Mn_3O_4 is insoluble at neutral pH. After cell internalization of Lipo-MGN, Mn^{2+} ions are released in endosomes where pH is low and lead to generating strong T1 MRI contrast (Chen et al. 2012; Bennewitz et al. 2011; Wang et al. 2015; Kim et al. 2011; Duan et al. 2018; Shapiro and Koretsky 2008).

The main functionality of manganese oxide in liposomes is to generate oxygen and convert hypoxic cancer cells to normoxic cells to make them susceptible to radiotherapy. To prove this hypothesis, a hypoxia assay was performed at different concentrations. The results showed decreasing fluorescent intensity corresponding to increasing oxygen concentration in cells, which is the result of the bio-reductive process that occurs with the hypoxia-sensitive agent in the assay (Takahashi et al. 2012). The effect of normoxia in cancer cells is the inability of cancer cells to repair themselves in the event of radiation, which makes them more susceptible to cell apoptosis (Zhang et al. 2019).

To show the anticancer effect of Lipo-MGNs in cancer cells after radiation, we conducted live/dead assays using the FDA/PI staining method. As predicted, the cells irradiated with 10 Gy showed almost 100% cell death compared to the 3 Gy, control and Lipo-MGN-only groups. As we confirmed HepG2 cell death with more than 3 Gy irradiation, we continued in vivo radiotherapy at a dose of 6 Gy single-dose after injecting Lipo-MGN. After 21 days, we observed a significant tumor reduction compared to the control. Single-dosage radiotherapy can benefit patients with fewer hospital visits and more effective recovery from cancer (Greco et al. 2021).

Our in vivo RT result using 6 Gy radiation is comparable to polymer lipid hydrophilic terpolymer–protein–MnO_2 nanoparticles, where 10 Gy of single-dose radiation was applied to achieve a 40% tumor recovery rate (Abbasi et al. 2016). Similar to our study, Mn_3O_4 was used for cancer therapy in the form of Mn_3O_4@Au-dsDNA/DOX, where dsDNA is used to activate the interferon gene pathway and doxorubicin (DOX) is chemotherapeutic. When combined with chemotherapy, immunotherapy exhibits strong anticancer efficacy by preventing tumor growth and extending in vivo survival times (Zhou et al. 2020). Tumor microenvironment modulation by DMn_3O_4-loaded nanoparticles can also improve therapeutic efficacy by triggering CTL-mediated antitumor immunity, which was seen in the case of hollow-MnO_2-PEG nanoparticles and doxorubicin-loaded alginate nanogel containing Mn^{2+} ions (Yang et al. 2017; Su et al. 2022; Zhou et al. 2022). To improve the tumor reduction effect of hypoxia-attenuating nanoparticle stimuli-responsive drug or gene release system can be introduced like in the case of siRNA-loaded hypoxia-sensitive micelleplex which is made from oligoethylenimine which is crosslinked with hypoxia breakable azobenzene (Li et al. 2022). Nitroimidazole is also a hypoxia stimuli-responsive linker which was used to release camptothecin from polymer-based micelle to treat HeLa cells (Zhou et al. 2021).

Overall manganese oxide nanoparticle-based nanosystems have high potential for therapy owing to catalytic reactivity with H_2O_2, increasing O_2 level in tumor environment. But in order to bring MGN-based nanosystem in clinical scenario, there must be a deeper study to understand the chemical reactivity(Bonet-Aleta et al. 2022) and long-term exposure study to analyze oxidative stress effect in different organ system such as neuronal cells (Alarifi et al. 2017).

In conclusion, we have developed biocompatible Lipo-MGN nanoparticles capable of attenuating hypoxia and treatment of hypoxic, radioresistant HepG2 cancer, along with enhanced MRI T1 contrast imaging capability.

Abbreviations

PEG	Polyethylene glycol
MGN	Manganese oxide nanoparticle
Lipo-MGN	MGN-loaded PEGylated liposomes
EDX	Energy dispersive X-ray
TGA	Thermogravimetric analysis
ICP-AES	Inductively coupled plasma atomic emission spectroscopy
HepG2	Human liver cancer cell line
MTS	(3-(4,5-Dimethylthiazol-2-yl)-5-(3-carboxymethoxyphenyl)-2-(4-sulfophenyl)-2*H*-tetrazolium)
DSPE-PEG	1,2-Distearoyl-sn-glycero-3-phosphoethanolamine
DPPC	Dipalmitoylphosphatidylcholine
TEM	Transmission electron microscope
cDNA	Complementary deoxyribonucleic acid
FDA	Fluorescein diacetate
PI	Propidium iodide
HIF-1α	Hypoxia-inducible factor 1-alpha

Supplementary Information

The online version contains supplementary material available at https://doi.org/10.1186/s12645-023-00182-x.

Additional file 1. Fig.S1 In vitro oxygen release study of Lipo-MGNs. Bubbles are generated due to oxygen release visible in the picture. **Fig.S2** T1 relaxation time, R1 relaxation rate and r1 relaxivity data of Lipo-MGN at different H_2O_2 concentrations and pH values. **Fig.S3** Survival of mice after radiotherapy. **Fig. S4** In vivo mice weight after radiotherapy.

Acknowledgements
Not applicable.

Author contributions
R.G.T. and S.K. contributed to the study concept, study design, data interpretation, and drafting of the manuscript. V.V., A.M., I.-K.P. contributed to the study design and material synthesis. Y.Y.J. contributed to the study design, data interpretation, review and drafting of the manuscript. R.N. helped in figure preparation. M.S.Y. facilitated radiation experiments. All authors read and approved the final manuscript.

Funding
This research was supported by the Bio and Medical Technology Development of the National Research Foundation (NRF) and funded by the Korean government (MSIT), No. 2019M3E5D1A02068082.

Availability of data and materials
All data and materials are available from the corresponding author on request.

Declarations

Ethics approval and consent to participate
BALB/c nude mice were acquired from Jungang Lab Animal Inc., Korea. The animal experiment was conducted in agreement with the National Institutes of Health Guide for the Care and Use of Laboratory Animals and approved by the Chonnam National University Medical School Research Institutional Animal Care and Use Committee (CNU IACUC-H-2019-6).

Consent for publication
Not applicable.

Competing interests
The authors declare that they have no competing interests.

Received: 14 October 2022 Accepted: 21 March 2023
Published online: 16 May 2023

References

Abbasi AZ, Gordijo CR, Amini MA, Maeda A, Rauth AM, DaCosta RS, Wu XY (2016) Hybrid manganese dioxide nanoparticles potentiate radiation therapy by modulating tumor hypoxia. Cancer Res 76:6643–6656
Alarifi S, Ali D, Alkahtani S (2017) Oxidative stress-induced DNA damage by manganese dioxide nanoparticles in human neuronal cells. Biomed Res Int 2017:5478790
Bennewitz MF, Lobo TL, Nkansah MK, Ulas G, Brudvig GW, Shapiro EM (2011) Biocompatible and pH-sensitive PLGA encapsulated MnO nanocrystals for molecular and cellular MRI. ACS Nano 5:3438–3446
Bonet-Aleta J, Calzada-Funes J, Hueso JL (2022) Manganese oxide nano-platforms in cancer therapy: recent advances on the development of synergistic strategies targeting the tumor microenvironment. Appl Mater Today 29:101628
Cai X, Zhu Q, Zeng Y, Zeng Q, Chen X, Zhan Y (2019) Manganese oxide nanoparticles as MRI contrast agents in tumor multimodal imaging and therapy. Int J Nanomed 14:8321–8344
Chen C, Lou T (2017) Hypoxia inducible factors in hepatocellular carcinoma. Oncotarget 8:46691–46703
Chen Y, Yin Q, Ji X, Zhang S, Chen H, Zheng Y, Sun Y, Qu H, Wang Z, Li Y et al (2012) Manganese oxide-based multifunctionalized mesoporous silica nanoparticles for pH-responsive MRI, ultrasonography and circumvention of MDR in cancer cells. Biomaterials 33:7126–7137
Choi HS, Mathew AP, Uthaman S, Vasukutty A, Kim IJ, Suh SH, Kim CS, Ma SK, Graham SA, Kim SW et al (2022) Inflammation-sensing catalase-mimicking nanozymes alleviate acute kidney injury via reversing local oxidative stress. J Nanobiotechnol 20:205
Duan B, Wang D, Wu H, Xu P, Jiang P, Xia G, Liu Z, Wang H, Guo Z, Chen Q (2018) Core–shell structurized Fe_3O_4@C@MnO_2 nanoparticles as pH responsive T1–T2* dual-modal contrast agents for tumor diagnosis. ACS Biomater Sci Eng 4:3047–3054
Elbanna M, Chowdhury NN, Rhome R, Fishel ML (2021) Clinical and Preclinical Outcomes of Combining Targeted Therapy With Radiotherapy. Front Oncol 11:749496
Gale EM, Atanasova IP, Blasi F, Ay I, Caravan P (2015) A manganese alternative to gadolinium for MRI contrast. J Am Chem Soc 137:15548–15557
Greco C, Pares O, Pimentel N, Louro V, Santiago I, Vieira S, Stroom J, Mateus D, Soares A, Marques J et al (2021) Safety and efficacy of virtual prostatectomy with single-dose radiotherapy in patients with intermediate-risk prostate cancer: results from the PROSINT phase 2 randomized clinical trial. JAMA Oncol 7:700–708
Ijaz Dar G, Iqbal MZ, Akakuru OU, Yao C, Awiaz G, Wu A (2020) Facile synthesis of Au@Mn3O4 magneto-plasmonic nanoflowers for T1-weighted magnetic resonance imaging and photothermal therapy of cancer. J Mater Chem B 8:8356–8367
Jain P, Bhagat S, Tunki L, Jangid AK, Singh S, Pooja D, Kulhari H (2020) Serotonin-stearic acid bioconjugate-coated completely biodegradable Mn_3O_4 nanocuboids for hepatocellular carcinoma targeting. ACS Appl Mater Interfaces 12:10170–10182
Kim T, Cho E-J, Chae Y, Kim M, Oh A, Jin J, Lee E-S, Baik H, Haam S, Suh J-S et al (2011) Urchin-shaped manganese oxide nanoparticles as pH-responsive activatable T1 contrast agents for magnetic resonance imaging. Angew Chem Int Ed 50:10589–10593
Li X, Xu X, Huang K, Wu Y, Lin Z, Yin L (2022) Hypoxia-reinforced antitumor RNA interference mediated by micelleplexes with programmed disintegration. Acta Biomater 148:194–205
Park S, Yoon WS, Rim CH (2020) Indications of external radiotherapy for hepatocellular carcinoma from updated clinical guidelines: diverse global viewpoints. World J Gastroenterol 26:393–403
Prasad P, Gordijo CR, Abbasi AZ, Maeda A, Ip A, Rauth AM, DaCosta RS, Wu XY (2014) Multifunctional albumin–MnO_2 nanoparticles modulate solid tumor microenvironment by attenuating hypoxia, acidosis, vascular endothelial growth factor and enhance radiation response. ACS Nano 8:3202–3212
Sayan M, Yegya-Raman N, Greco SH, Gui B, Zhang A, Chundury A, Grandhi MS, Hochster HS, Kennedy TJ, Langan RC et al (2019) Rethinking the role of radiation therapy in the treatment of unresectable hepatocellular carcinoma: a data driven treatment algorithm for optimizing outcomes. Front Oncol. https://doi.org/10.3389/fonc.2019.00345
Shapiro EM, Koretsky AP (2008) Convertible manganese contrast for molecular and cellular MRI. Magn Reson Med 60:265–269
Shin SW, Jung W, Choi C, Kim SY, Son A, Kim H, Lee N, Park HC (2018) Fucoidan-manganese dioxide nanoparticles potentiate radiation therapy by Co-targeting tumor hypoxia and angiogenesis. Mar Drugs 16(2):510
Song M, Liu T, Shi C, Zhang X, Chen X (2016) Bioconjugated manganese dioxide nanoparticles enhance chemotherapy response by priming tumor-associated macrophages toward M1-like phenotype and attenuating tumor hypoxia. ACS Nano 10:633–647
Sorensen BS, Horsman MR (2020) Tumor hypoxia: impact on radiation therapy and molecular pathways. Front Oncol 10:562
Su M, Zhu Y, Chen J, Zhang B, Sun C, Chen M, Yang X (2022) Microfluidic synthesis of manganese-alginate nanogels with self-supplying H_2O_2 capability for synergistic chemo/chemodynamic therapy and boosting anticancer immunity. Chem Eng J 435:134926
Takahashi S, Piao W, Matsumura Y, Komatsu T, Ueno T, Terai T, Kamachi T, Kohno M, Nagano T, Hanaoka K (2012) Reversible off-on fluorescence probe for hypoxia and imaging of hypoxia–normoxia cycles in live cells. J Am Chem Soc 134:19588–19591
Wang X, Niu D, Wu Q, Bao S, Su T, Liu X, Zhang S, Wang Q (2015) Iron oxide/manganese oxide co-loaded hybrid nanogels as pH-responsive magnetic resonance contrast agents. Biomaterials 53:349–357

Xu G, Jin B, Xian X, Yang H, Zhao H, Du S, Makuuchi M, Pawlik TM, Mao Y (2021) Evolutions in the management of hepatocellular carcinoma over last 4 decades: an analysis from the 100 most influential articles in the field. Liver Cancer 10:137–150

Yang G, Xu L, Chao Y, Xu J, Sun X, Wu Y, Peng R, Liu Z (2017) Hollow MnO2 as a tumor-microenvironment-responsive biodegradable nano-platform for combination therapy favoring antitumor immune responses. Nat Commun 8:902

Yao J, Cheng Y, Zhou M, Zhao S, Lin S, Wang X, Wu J, Li S, Wei H (2018) ROS scavenging Mn(3)O(4) nanozymes for in vivo anti-inflammation. Chem Sci 9:2927–2933

Zhang C, Yan L, Gu Z, Zhao Y (2019) Strategies based on metal-based nanoparticles for hypoxic-tumor radiotherapy. Chem Sci 10:6932–6943

Zhou M, Wang X, Lin S, Cheng Y, Zhao S, Lin J, Fang Z, Lou Z, Qin L, Wei H (2020) Multifunctional STING-activating Mn_3O_4 @Au-dsDNA/DOX nanoparticle for antitumor immunotherapy. Adv Healthc Mater 9:e2000064

Zhou Q, Mohammed F, Wang Y, Wang J, Lu N, Li J, Ge Z (2021) Hypoxia-responsive block copolymer polyprodrugs for complementary photodynamic-chemotherapy. J Control Release 339:130–142

Zhou Z, Huang J, Zhang Z, Zhang L, Cao Y, Xu Z, Kang Y, Xue P (2022) Bimetallic PdPt-based nanocatalysts for photothermal-augmented tumor starvation and sonodynamic therapy in NIR-II biowindow assisted by an oxygen Self-Supply strategy. Chem Eng J 435:135085

Publisher's Note